SINERGI Vol. 30, No. 1, February 2026: 273-286
http://publikasi.mercubuana.ac.id/index.php/sinergi
http://doi.org/10.22441/sinergi.2026.1.025

Stress-strain behavior and residual strength of Petobo sand with variable fines content under consolidated undrained triaxial loading

Desiana Vidayanti[1,2*], Paulus Pramono Rahardjo[1], Ramli Nazir[1,3]
[1]Department of Civil Engineering, Parahyangan Catholic University, Indonesia
[2]Department of Civil Engineering, Mercu Buana University, Indonesia
[3]Centre of Tropical Geoengineering, Universiti Teknologi Malaysia, Malaysia

Abstract
Liquefaction was one of the primary causes of severe ground deformation during the 2018 Palu earthquake, particularly in the Petobo area, where large-scale flow liquefaction resulted in extensive ground displacement. Despite extensive field investigations, laboratory-based residual shear strength data for Petobo soil had not been available to explain the exceptional mobility of the flowslide. This study investigated the stress-strain response and post-liquefaction residual strength of Petobo silty sand with variable fines content using monotonic consolidated undrained (CU) triaxial tests. Reconstituted specimens were prepared using the moist tamping method with fines contents of approximately 9% and 26.4% and tested under three levels of initial mean effective stress. The results showed that specimens with higher fines content generated excess pore water pressure more rapidly and exhibited stronger contractive behavior at small strains. At large strains, however, both fines contents mobilized comparable residual strength levels, expressed as normalized residual strength ratios (q_{res}/p'_0) ranging from 0.79 to 0.94. These findings indicate that while fines content influenced early-stage contractive behavior and pore-pressure generation, its effect on post-liquefaction residual strength under very loose density conditions was limited. The residual shear resistance was primarily governed by the loose sand fabric and the effective stress level at the stabilized post-peak condition. This study provides the first laboratory-based residual shear strength data for Petobo silty sand, offering essential parameters for back-analysis, numerical modeling, and liquefaction hazard assessment related to flow-type deformation in Palu and similar alluvial environments.

Keywords:
Fines content;
Liquefaction;
Palu;
Residual strength;
Silty sand;

Article History:
Received: October 4, 2025
Revised: December 14, 2025
Accepted: January 17, 2026
Published: January 25, 2026

Corresponding Author:
Desiana Vidayanti,
Department of Civil Engineering, Parahyangan Catholic University, Bandung, Indonesia.
Department of Civil Engineering, Mercu Buana University, Jakarta, Indonesia
Email:
Desiana Vidayanti:
desianavidayanti@gmail.com

INTRODUCTION

Liquefaction is one of the primary causes of severe infrastructure damage during major earthquakes. During the 2018 Palu earthquake, the Petobo area experienced one of the most destructive cases of flow liquefaction ever recorded, resulting in large-scale ground displacement and the devastation of residential areas and public facilities [1, 2, 3]. This event involved complex subsurface mechanisms, including confined aquifers, stratified layers, and undissipated pore-pressure migration [4][5] thereby highlighting the need for detailed laboratory investigation of the affected soils.

Although the Petobo flowslide has been widely studied from geomorphological, hydrological, and stratigraphic perspectives [1, 6, 7, 8] no published study has reported laboratory measurements of post-liquefaction residual shear

strength for Petobo soil. Residual strength governs the runout distance of liquefied masses and represents a critical mechanical parameter controlling whether deformation stabilizes or evolves into catastrophic flow failure. The absence of site-specific residual strength data has therefore limited the reliability of back-analyses and hazard assessment in the Palu region.

In general, loose saturated sands are highly susceptible to liquefaction due to their contractive behavior, rapid pore-pressure buildup, and consequent loss of effective stress [9, 10, 11]. The presence of fine particles further complicates this response. Non-plastic fines at low contents may accelerate pore-pressure generation and reduce liquefaction resistance, whereas higher fines contents can enhance packing density and partially improve resistance [12]–[16]. In addition, confining stress, particle morphology, and soil fabric are known to influence the undrained response of silty sands [17]–[21].

Beyond liquefaction initiation, fines content also affects post-liquefaction behavior by modifying soil packing and contact fabric. For very loose sands, post-liquefaction residual strength is typically low and primarily governed by the looseness of the sand skeleton, while fines tend to influence contractive tendency and the rate of strength degradation rather than producing a systematic increase in residual strength. A large proportion of previous liquefaction studies has focused on cyclic loading relevant to triggering mechanisms[22][23]. In contrast, post-liquefaction residual shear strength controlling large-deformation behavior and flow mobility is more appropriately evaluated using monotonic undrained loading [24].

Concepts from critical-state and steady-state soil mechanics provide a useful qualitative framework for interpreting stress-path stabilization and residual strength mobilization at large strains under undrained loading. Experimental studies on silty sands from various geological settings have reported a wide range of post-liquefaction residual strengths, reflecting the influence of material characteristics, fines content, and initial density [25][26]. However, laboratory measurements of post-liquefaction residual shear strength for Petobo silty sand remain unavailable to date [27].

Within this context, the present study addresses the following research question: to what extent does fines content influence the normalized post-liquefaction residual shear strength of very loose Petobo silty sand under undrained loading, and how does this behavior relate to the long-runout flow deformation observed during the 2018 Palu event?

The objective of this study is to provide laboratory-based residual shear strength data for Petobo soil, quantify the influence of fines content under very loose density conditions, and offer mechanistic insight into the 2018 flowslide. The findings provide essential input for back-analysis, numerical modeling, and liquefaction hazard assessment in Palu and similar alluvial environments.

State-of-the-Art Comparison and Novelty

Previous studies on liquefaction-induced flow failures have addressed cyclic loading behavior, liquefaction triggering, and flow mechanisms primarily through field case histories, numerical back-analyses, centrifuge modeling, and cyclic laboratory tests [1, 3, 7, 8, 28, 29]. Within soil mechanics research, undrained monotonic tests have been widely employed to investigate steady-state or critical-state behavior of clean sands and silty sands, often using idealized or reconstituted materials and focusing on constitutive modeling or state-parameter characterization rather than on experimentally measured residual strength directly applicable to documented flow failures [27][30]–[33].

In contrast to these studies, laboratory investigations providing directly measured post-liquefaction residual shear strength of natural silty sands from documented long-runout flow-liquefaction sites remain limited. In particular, consolidated undrained monotonic triaxial measurements of residual strength for Petobo silty sand have not been reported in the published literature, despite its central role in the long-runout flow deformation during the 2018 Palu earthquake

The novelty of the present study lies in providing the first direct laboratory-measured post-liquefaction residual shear strength data for Petobo silty sand obtained from controlled consolidated undrained monotonic triaxial tests, explicitly addressing the influence of fines content under very loose density conditions. By focusing on large-strain residual strength rather than liquefaction triggering, the study bridges the gap between laboratory soil mechanics and back-analysis of the long-runout flow failures observed during the 2018 Palu event.

METHOD

In this study, residual strength was evaluated directly from monotonic consolidated undrained (CU) triaxial tests at large strains. Critical-state soil mechanics concepts were used only at a qualitative level to interpret the tendency toward post-peak stabilization and steady stress response under undrained loading.

.

Material

The soil samples were collected from the Petobo Sub-district, Palu City, one of the areas most severely affected by liquefaction during the 28 September 2018 earthquake. The Petobo area experienced large-scale flow liquefaction with a runout distance of approximately 2.1 km, resulting in massive ground displacement and widespread destruction of residential areas.

The tested soils were obtained from a loose sand layer near the ground surface within the flow-affected zone. Two types of samples were collected to represent different fines contents and geomorphological settings within the Petobo flowslide area

The low-fines sample (TG, FC = 9%) was collected from a drainage dike location corresponding to the upstream initiation zone of the flow liquefaction. The high-fines sample (AP, FC = 26.4%) was collected from a residential area within the main flow-affected zone that experienced extensive lateral spreading and large ground displacement.

An overview of the affected area and sampling locations is shown in Figure 1. Throughout this paper, TG and AP denote samples collected from the drainage dike (*Tanggul Saluran*) and residential area (*Area Perumahan*), respectively. The numerical suffix (1-3) indicates the level of initial mean effective stress applied during consolidation (100, 150, and 200 kPa).

Figure 1. Sampling locations in Petobo: (a) drainage dike (Location A), (b) area affected by massive ground flow (Location B), (c) overview of the flow liquefaction-affected zone

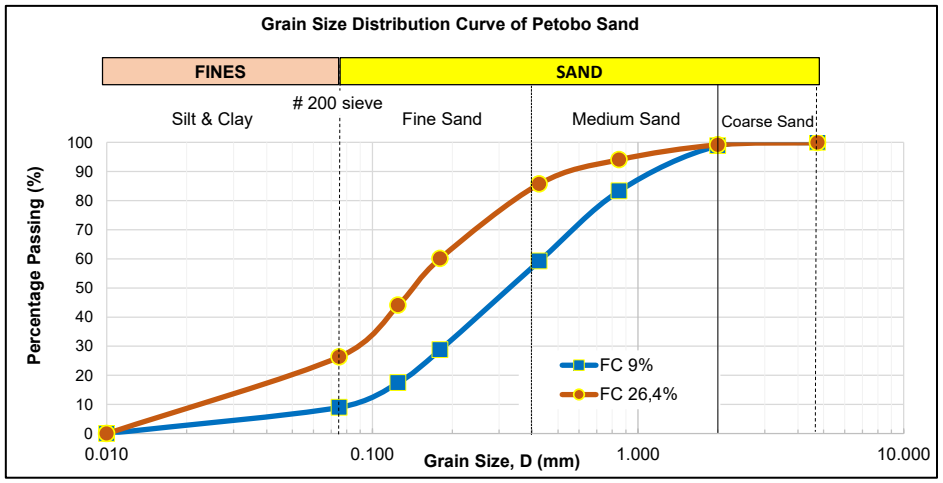

Figure 2. Grain size distribution of soil samples with fines content of 9% and 26.4%

Soil Characterization

The index properties of the soil were determined using standard ASTM and SNI procedures, including grain size distribution (ASTM D6913 for sieve analysis, ASTM D7928 for hydrometer analysis, and SNI 3423:2008), specific gravity (ASTM D854), maximum and minimum index densities (ASTM D4253 and ASTM D4254), Atterberg limits (ASTM D4318), and natural water content (ASTM D2216). The grain size distribution curves were presented in Figure 2, and the index properties were summarized in Table 1.

Table 1. Index properties of Petobo sand samples with fines contents of 9% and 26.4%

Index Properties	Sample A	Sample B
Gs	2.7	2.69
Gravel (%)	0	0
Coarse Sand (%)	1.17	0.09
Medium Sand (%)	39.58	13
Fine Sand (%)	50.25	59
Fines Content	9.01	26.37
D_{50} (mm)	0.32	0.15
D_{10} (mm)	0.08	0.02
D_{30} (mm)	0.18	0.09
D_{60} (mm)	0.35	0.18
Cc	1.23	2.05
Cu	4.67	8.18
PL (%)	NP	20.65
PI (%)	0	13.65
Soil Classification (USCS)	SP - SM	SC
$\rho_{d\,max}$ (Mgr/cm^3)	1.48	1.60
$\rho_{d\,min}$ (Mgr/cm^3)	1.20	1.22
e_{max}	1.250	1.209
e_{min}	0.821	0.680

Two groups of soils were identified:

1. Low-fines sand (TG, FC = 9%), approaching clean sand, obtained from Location A (Figures 1a and 1c).
2. High-fines sand (AP, FC = 26.4%) classified as SC according to the Unified Soil Classification System (USCS). However, based on visual observation and mechanical behavior, this soil more closely resembles silty sand. It was obtained from Location B (Figures 1b and 1c).

Specimen Preparation

Six cylindrical specimens (38 mm in diameter and 76 mm in height) were prepared: three TG specimens (FC = 9%) and three AP specimens (FC = 26.4%), each tested under initial mean effective stresses of 100, 150, and 200 kPa.

All specimens were prepared in a very loose condition, with relative densities ranging from approximately 11% to 20%, consistent with the loose fabric observed in the field. This preparation aimed to promote contractive behavior and allow convergence toward a stabilized post-peak condition during monotonic undrained loading.

The moist tamping (undercompaction) method (Figure 3), originally proposed by Ladd and widely recommended for silty sands [33][34] was adopted because it enabled very loose specimen preparation representative of post-liquefaction conditions, minimized fines segregation, and was more practical than air pluviation or slurry deposition

Figure 3. Specimen preparation using the moist tamping (undercompaction) method

Consolidated Undrained (CU) Triaxial Test Procedure

Monotonic Consolidated Undrained (CU) triaxial compression tests were conducted in accordance with ASTM D4767 (2011) and SNI 03-2455:1991 (Figure 4). The CU test was selected because it simulated the undrained behavior of saturated soils under axial loading and allowed measurement of excess pore water pressure (Δu), deformation, and the effective stress path ($p' - q$)

The testing procedure consisted of the following stages:

Saturation stage

The specimens were saturated by applying back pressure until the Skempton parameter (B-value) reached ≥ 0.95. This step was essential to ensure full saturation so that any volume change was entirely governed by pore water pressure. Ensuring full saturation and consistent test repeatability aligned with recommended laboratory procedures for obtaining reliable large-strain behavior in triaxial testing [33].

Isotropic consolidation stage

Once saturation was achieved, the specimens were isotropically consolidated under initial mean effective stresses (p'_0) of 100, 150, and 200 kPa. These stress levels simulated different in-situ effective stress conditions corresponding to soil depth. This stress range reflected the effective stress conditions of the upper 5-10 m of the Petobo deposit, which corresponded to the zone where liquefaction triggering and flow deformation were observed during the 2018 Palu event.

Monotonic shearing stage

The specimens were axially loaded under strain-controlled conditions at a constant rate of 0.05 mm/min. The tests were continued until axial strains exceeded 20% to ensure that the soil specimens reached a stabilized post-peak stress condition, which is conceptually consistent with a critical-state-like response at large strains.

During the shearing stage, drainage was prevented, and excess pore-water pressure was continuously measured, confirming undrained conditions

Repeatability and Error Control

Each test condition was performed at least twice to verify repeatability. Differences in peak and residual deviator stresses remained within ±5%, which is consistent with widely accepted laboratory practice for monotonic triaxial testing of natural sands, as reported in recent experimental studies [24][27]. Average values from the repeated tests were used in the analysis, and any test showing deviations beyond this threshold was excluded. The consistent trends confirm that the measured stress-strain response and residual strength are representative and reliable

Figure 4. Consolidated Undrained (CU) triaxial compression test apparatus

Test Data and Graphical Results

The CU tests produced the following curves:

1. stress-strain curves $(q - \varepsilon)$,
2. excess pore water pressure development $(\Delta u - \varepsilon)$, and
3. effective stress paths $(p' - q)$.

Parameter Calculation

1. **Deviator stress (q):**
   $q = (\sigma'_1 - \sigma'_3)$ (1)
   where σ'_1 and σ'_3 were the major and minor effective principal stresses, respectively.
   This parameter represented the mobilized shear stress in the specimen and quantified the shear resistance developed during undrained shearing.
2. **Mean effective stress (p'):**
   $p' = \frac{1}{3}(\sigma'_1 + 2\sigma'_3)$ (2)
   This parameter represented the average effective stress carried by the soil skeleton after accounting for pore-water pressure and was used to construct the effective stress path.
3. **Excess pore water pressure (Δu):**
   The excess pore water pressure, Δu, represented the pore pressure generated during axial loading. It was continuously recorded to illustrate the mechanism of effective stress reduction and to identify the tendency toward contractive or dilative soil response.

These parameters were computed at each loading increment to capture the evolution of stress and pore-pressure during undrained shearing

Justification for Using Monotonic CU Triaxial Tests

Although liquefaction in the field is a cyclic phenomenon, cyclic triaxial tests were often difficult to control at large strains because very loose silty sands rapidly lost stiffness and could reach instability before a residual condition was achieved [9]. Monotonic undrained triaxial tests overcame this limitation by allowing continuous shearing to large strains, thereby enabling direct measurement of residual or steady-state shear strength under a controlled stress path [25].

This approach has long been used for post-liquefaction characterization and has continued to be supported by recent studies showing that monotonic and cyclic responses can be interpreted consistently within modern critical-state-based or equivalent-state conceptual frameworks [30][32]. Updated laboratory recommendations have further emphasized the suitability of controlled monotonic shearing for obtaining reliable large-strain strength characteristics in cohesionless soils [33]. Based on these considerations, the monotonic Consolidated Undrained (CU) triaxial test was selected to evaluate the post-liquefaction residual behavior of Petobo silty sand using a critical-state, informed qualitative interpretation.

Data Analysis

In this study, concepts from critical-state soil mechanics are invoked solely as a qualitative interpretative framework to describe stress stabilization at large strains under undrained loading. No attempt is made to establish a Critical State Line in $e - log\ p'$ space or to evaluate state parameters, as the focus of the study is the experimental quantification of post-liquefaction residual strength, rather than formal state characterization or constitutive modeling. Accordingly, the term “critical state” is used herein in a descriptive mechanical sense, referring to a steady post-peak stress condition observed experimentally.

From a critical-state perspective, soil behavior is governed primarily by void ratio and effective stress. In the present experimental study, relative density (Dr) is therefore used only as a practical descriptor of the initial void ratio condition of the specimens and is not treated as a fundamental state variable. Under undrained loading, this initial condition manifests through stress-path evolution and excess pore-water pressure generation, leading to a contractive response and post-peak stabilization.

The experimental results were interpreted based on the observed stress-strain response and pore pressure evolution under undrained loading conditions. The analysis focused on the evolution of deviator stress (q), mean effective stress (p') and excess pore water pressure (Δu) during monotonic shearing, from initial loading through post-peak behavior until a stable response was reached at large strains. This stable post-peak condition was taken to represent the residual shear strength of the soil.

Definition of Residual Strength and Steady Post-Peak Condition

In this study, the term steady post-peak condition refers to an experimentally observed stabilized stress response at large strains under undrained loading, identified from the convergence of stress-strain behavior and effective stress paths. This condition is mechanically consistent with what is commonly described in the literature as a steady-state or critical-state-like condition, but is used here strictly in a descriptive sense, without implying formal

critical state characterization, uniqueness of a critical state locus, or evaluation of state parameters. The term residual strength denotes the magnitude of shear resistance mobilized under this stabilized post-peak condition.

Determination of Residual Strength (q_{res})

Residual strength (q_{res}) was defined as the average deviator stress measured over the large-strain plateau region, typically observed at axial strains of about 15-20% or greater, once a steady post-peak condition was reached. In the present tests, stable residual conditions were attained at axial strains exceeding approximately 30%, where both deviator stress (q) and mean effective stress (p') approached near-constant values under undrained monotonic loading. This strain threshold was identified directly from the experimental stress-strain responses, as stabilization was not observed at lower strains.

No attempt was made to establish a formal critical state line in $e - log\ p'$ space or to evaluate the state parameter, as the objective of this study was not state characterization or constitutive modeling. Instead, the focus was placed on experimentally observed residual strength and its relevance to post-liquefaction stability and flow deformation in loose silty sand.

The influence of fines content on stress-strain evolution and the resulting residual strength was evaluated to elucidate the post-liquefaction behavior of Petobo silty sand

RESULTS AND DISCUSSION

As stated earlier, concepts from critical-state soil mechanics were employed only as a qualitative interpretative framework to describe stress-path stabilization and residual strength mobilization at large strains, including the attainment of a steady post-peak (steady-state-like) without attempting state-based soil characterization or constitutive modeling.

Table 2. Summary of CU triaxial test results

Fine Content (FC %)	p'_0 (kPa)	q_{max} (kPa)	Δu (kPa)	(q_{res}) (kPa)	q_{res}/p'_0
9	100	106.13	62.10	89.47	0.89
9	150	134.36	95.40	126.91	0.85
9	200	186.62	123.20	177.73	0.89
26.4	100	104.75	62.35	93.54	0.94
26.4	150	130.21	102.00	118.30	0.79
26.4	200	190.04	127.60	178.12	0.89

The results of the CU triaxial tests on Petobo sand were summarized in Table 2, which presented the maximum deviator stress (q_{max}), maximum excess pore water pressure (Δu_{max}), and residual strength for the two fines contents (9% and 26.4%) under three levels of confining stress, or initial mean effective stress (p'_0 = 100, 150, and 200 kPa). The corresponding stress-strain ($q-\varepsilon$), pore-pressure-strain ($\Delta u-\varepsilon$), and and effective stress path ($p'-q$) responses were illustrated in Figures 5-7

Stress-Strain Behavior ($q-\varepsilon$)

The stress-strain curves (Figure 5) exhibited a characteristic response of very loose silty sand, marked by a rapid increase in deviator stress at small strains followed by a broad plateau extending to large strains (ε > 30%). Pronounced strain softening was not observed; instead, deviator stress gradually approached a nearly constant level, indicating that the specimens attained a steady post-peak condition characterized by stabilized stress response at large strains.

The peak deviator stress (q_{max}) increased systematically with the initial mean effective stress (p'_0) reflecting the effect of consolidation level on peak resistance under undrained loading.

Differences in q_{max}, between the two fines contents were relatively small (generally within 1-5%), reflecting that at very loose densities (Dr = 11% for FC 9% and Dr = 20% for FC 26.4%), peak shear response is governed predominantly by the sand skeleton. The influence of fines content was more evident in pore-pressure generation and effective stress path curvature rather than in peak deviator stress.

The Petobo silty sand exhibited moderate post-peak behavior, with a gradual transition toward a stable post-peak condition rather than abrupt strain softening. This response is attributed to the combined effect of non-plastic fines and particle characteristics of the volcanic-derived material, which moderated the post-peak strength degradation. Nevertheless, all specimens mobilized low normalized residual strength ratios (q_{res}/p'_0= 0.79-0.94), indicating high susceptibility to flow-type deformation once liquefaction was triggered.

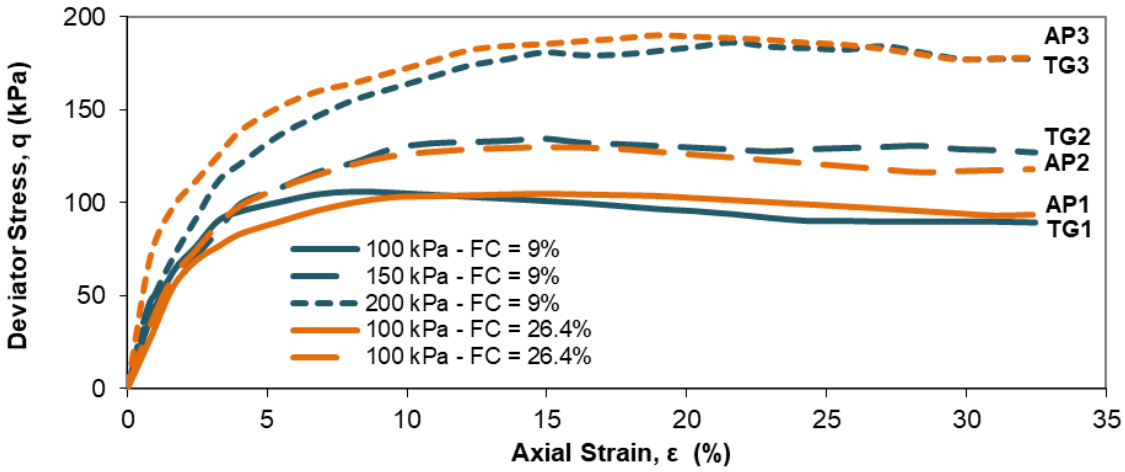

Figure 5. Stress-strain behavior of Petobo sand, expressed in terms of deviator stress (q) versus axial strain (ε), at fines contents of 9% and 26.4% under effective confining stresses of 100, 150, and 200 kPa. TG: drainage dike sample (FC = 9%); AP: residential area sample (FC = 26.4%).

Excess Pore Water Pressure Development $(\Delta u - \varepsilon)$

The $(\Delta u - \varepsilon)$ curves (Figure 6) showed a rapid increase in excess pore water pressure at small strains (<10%) for all specimens, indicating strongly contractive behavior typical of very loose sands. Both fines-content groups reached similar maximum excess pore-pressures Δu_{max} demonstrating that at very low relative densities the dominant factor governing pore-pressure buildup was the loose, compressible sand skeleton rather than fines content alone.

Specimens with 26.4% fines generated slightly higher Δu at intermediate strains, but the overall difference in Δu_{max} between the two fines contents remained modest (generally within 5%). This observation suggests that within the tested density range, fines content influences the rate and shape of pore-pressure development more strongly than its ultimate magnitude

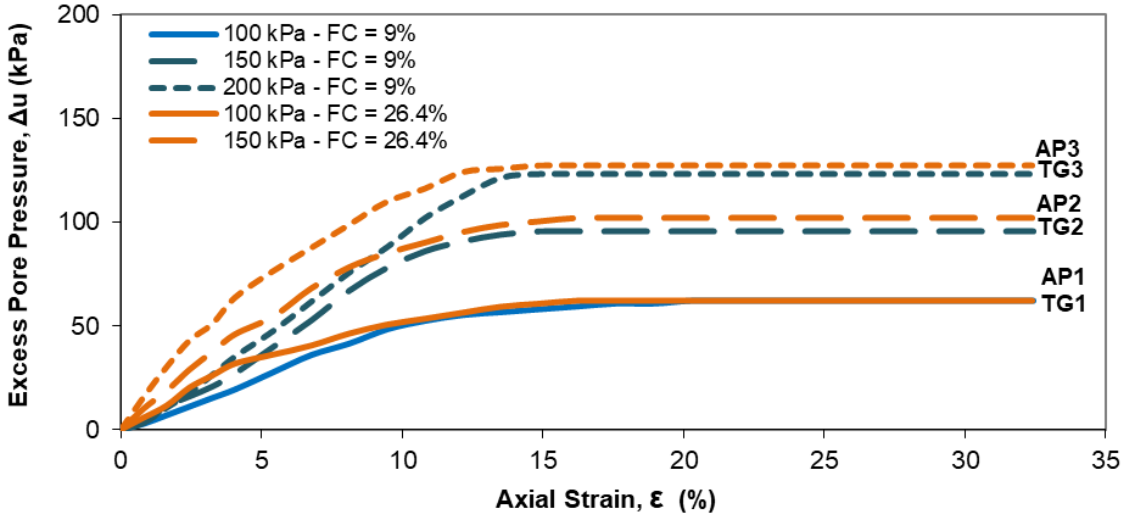

Figure 6. Excess pore water pressure-axial strain Δu_{max} behavior of Petobo sand with fines contents of 9% and 26.4% under effective confining stresses of 100, 150, and 200 kPa. TG denotes the drainage dike sample (FC = 9%), while AP denotes the residential area sample (FC = 26.4%)

Steady-State Stress Ratio under Undrained Loading

Under monotonic consolidated undrained (CU) loading, reconstituted Petobo silty sand specimens consistently approached a stable post-peak stress condition at axial strains of approximately 15-20%, at which both deviator stress (q) and mean effective stress (p') became nearly constant. The stress ratio (q/p') measured at this large-strain stage was used to characterize the post-peak stabilized response under undrained conditions.

The computed stress ratios showed good consistency within each fines-content group, with average values of approximately 1.31 for FC = 9% and 1.36 for FC = 26.4% (Table 3)

These values fall within ranges commonly reported for loose silty sands and volcanic-derived granular materials under undrained shearing. Previous studies indicate that fines content primarily influences contractive tendency and stress-path curvature rather than producing pronounced differences in the ultimate steady stress ratio at large strains, which is consistent with the present results.

Table 3. Summary of Steady Post-Peak Stress Ratio under Undrained Loading. The steady post-peak stress ratio (q/p') is defined as the stress ratio measured at large strains after stress stabilization under undrained loading, representing the post-peak residual response of the soil rather than a formally defined critical state.

Although the tests were conducted under controlled effective confining stresses, the evolution of mean effective stress during undrained shearing played a key role in governing the observed stress-strain response

Table 3. Summary of Steady Post-Peak Stress Ratio under Undrained Loading

Specimen	FC (%)	p'_0 (kPa)	$\frac{q}{p'}(Post\ Peak)$	Observed response
TG1	9	100	1.321	Cont
TG2	9	150	1.310	Cont
TG3	9	200	1.306	Cont
Average (FC = 9%)			**1.312**	
AP1	26.4	100	1.359	Cont
AP2	26.4	150	1.353	Cont
AP3	26.4	200	1.352	Cont
Average (FC = 26.4%)			**1.355**	

Note: Cont = contractive

Effective Stress Path $(p' - q)$

From a critical-state soil mechanics perspective, the contractive behavior summarized in Table 3 was interpreted based on the undrained effective stress-path response, without attempting a formal determination of the critical state line or state parameters. Under undrained loading, contractive behavior was characterized by a progressive reduction in mean effective stress accompanied by positive pore-water pressure generation, which was manifested by a downward-leftward $(p' - q)$ stress path at large strains (Figure 7)

The effective stress paths (Figure 7) consistently moved downward to the left, reflecting the progressive reduction in mean effective stress (p') associated with contractive behavior under undrained loading. Specimens with higher fines content shifted more rapidly toward lower p' at small strains, indicating greater excess pore water pressure generation. At larger strains, however, stress paths for both fines contents converged toward similar stabilized post-peak conditions

Although high-fines specimens were initially more contractive, they ultimately mobilized comparable or slightly higher normalized residual strength ratios (q_{res}/p'_0 = 0.79-0.94) compared with low-fines specimens (q_{res}/p'_0 = 0.85-0.89) (Table 2).

This behavior suggests that fines content enhances early-stage contractive response while potentially improving particle packing and interparticle contact at large strains. Overall, the influence of fines on liquefaction response is nonlinear, emphasizing the need to distinguish between liquefaction initiation susceptibility and post-liquefaction stability.

At large axial strains, the effective stress paths converged toward a stable post-peak condition, where both deviator stress (q) and mean effective stress (p') changed only marginally with continued straining, indicating mobilization of residual shear resistance under undrained loading.This interpretation is based on the observed stabilization of stress paths rather than on a formal determination of a critical state line or state parameters, while differences in fines content primarily influenced early-stage contractive behavior and pore-pressure generation.

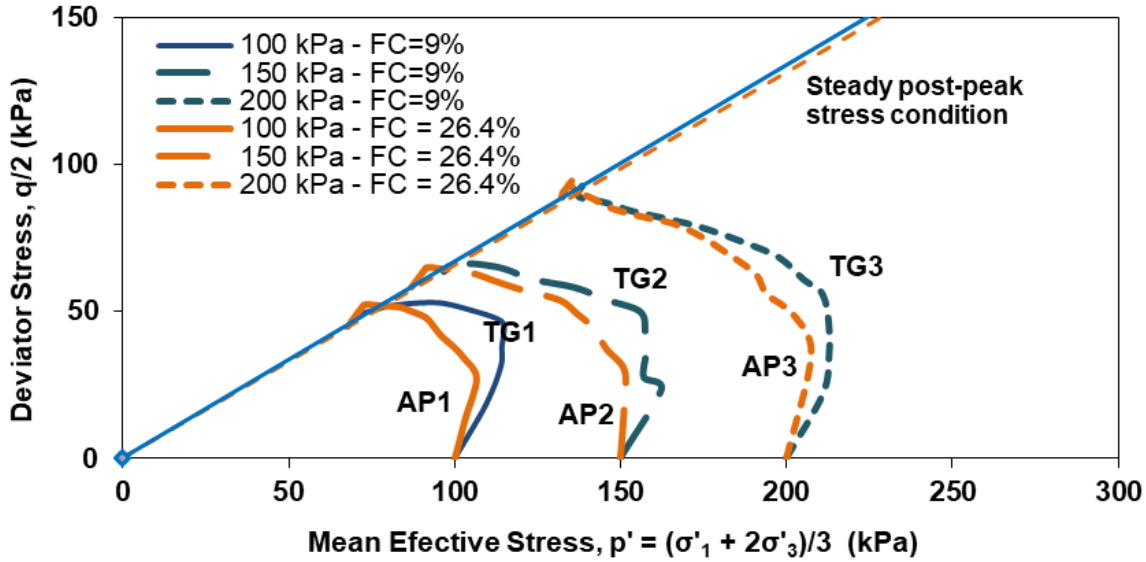

Figure 7. Effective stress paths $(p'-q)$ of Petobo sand with fines contents of 9% and 26.4% during undrained shearing under effective confining stresses of 100, 150, and 200 kPa. TG denotes the drainage dike sample (FC = 9%), while AP denotes the residential area sample (FC = 26.4%)

Empirical Relationship and Interpretation of Post-Peak Undrained Behavior and Residual Strength

The normalized residual strength ratio (q_{res}/p'_0) exhibited only minor variation between the two fines-content groups, with nearly identical average values of approximately 0.88. This result indicated that at very loose initial densities (Dr = 11-20%), fines content did not systematically control residual strength. Instead, post-liquefaction resistance was governed primarily by the loose sand skeleton and the effective stress level at the onset of steady post-peak shearing.

A simple linear regression was performed across all six specimens to examine the empirical relationship between fines content (FC) and normalized residual strength. The resulting relationship can be written as (3)

$$q_{res}/p'_0 = -0.00019 \cdot FC + 0.878 \quad (3)$$

As shown in (3), the regression exhibited a near-zero slope and a very low coefficient of determination, indicating that fines content was not a dominant predictor of residual strength under the very loose density conditions tested.

From a mechanical perspective, the limited influence of fines content on residual strength can be explained by the very loose initial packing condition of the specimens. Although relative density is commonly used to describe initial soil state, from a critical-state perspective soil behavior is governed by void ratio and effective stress rather than relative density alone. In this study, relative density serves only as a practical descriptor of the initial packing condition. Under such very loose conditions, fines primarily modify soil fabric and contractive tendency, which affects pore-pressure generation and the shape of the effective stress path during early stages of undrained shearing. However, once large strains are reached and a steady post-peak condition is attained, the residual strength is controlled mainly by the collapse of the loose sand skeleton and the effective stress level, resulting in similar normalized residual strength ratios despite differences in fines content.

Table 3 summarizes the steady post-peak stress ratios (q/p') identified from the large-strain portion of the effective stress paths. The measured ratios range from 1.306 to 1.359 and were similar for both fines contents, indicating convergence toward comparable stabilized post-peak stress conditions despite differences in early-stage contractive behavior. This similarity in stress ratios confirms that the specimens reached mechanically equivalent steady conditions, supporting the interpretation that fines content influenced the stress-path evolution rather than the ultimate residual strength.

Effect of Initial Mean Effective Stress (p'_0)

Increasing the initial mean effective stress from 100 to 200 kPa increased the absolute residual strength (q_{res} increased from approximately 90 kPa to 180 kPa for both fines contents); however, the normalized residual strength ratio (q_{res}/p'_0 = 0.85-0.89) did not increase proportionally. This stress-ratio dilution

effect is consistent with critical-state interpretations, in which higher initial effective stress increases absolute shear capacity without a corresponding increase in normalized post-peak strength.

This laboratory trend is consistent with field observations from Petobo, where deeper layers subjected to higher overburden stresses likely mobilized lower normalized residual strength ratios, while shallower loose layers experienced greater displacement and more extensive flow deformation during the 2018 event.

Comparison with Previous Studies

Previous studies have shown that the influence of fines content on liquefaction behavior depends strongly on the initial density and soil fabric. At comparable stress and density conditions, variations in fines content tend to have a limited effect on the undrained response, as the behavior is governed primarily by the overall stress-density state [19].

Dynamic centrifuge studies further indicate that non-plastic fines may increase liquefaction resistance in medium-dense sands, whereas their influence becomes less pronounced when soil behavior is controlled mainly by density and effective stress level [14]. Most of these studies focus on liquefaction triggering or failure mode transition rather than on the stabilized response at large strains.

In the present study, specimens were tested under very loose and constrained initial states. The results show that variations in fines content significantly affect the early-stage undrained response, particularly excess pore-water pressure generation and effective stress path evolution. However, once a stabilized post-peak condition is reached at large strains, the residual strength remains broadly comparable across the tested fines contents.

This indicates that post-liquefaction resistance under very loose conditions is governed predominantly by the overall stress–density state, with fines influencing mainly the stress-path development rather than the residual strength level.

Practical Implications for Back-Analysis and Engineering Assessment

The residual strength ratios obtained in this study provide practical input parameters for back-analysis and numerical modeling of liquefaction-induced flow deformation in Petobo and similar deposits. Previous numerical studies have demonstrated that predicted runout distances are highly sensitive to the assumed post-liquefaction residual strength. Accordingly, the experimentally derived values (q_{res}/p'_0 = 0.79-0.94) define a realistic lower-bound range for post-liquefaction resistance suitable for engineering analyses.

For typical effective stress levels in the shallow Petobo deposits (p'_0 = 100-200 kPa), the corresponding residual shear strengths (q_{res} = 90-180 kPa or $S_{u,res} = q_{res}/2$ = 45-90 kPa) represent the stress levels governing post-liquefaction mobility rather than peak resistance. These results indicate that assuming higher residual strength values based solely on fines content may lead to unconservative deformation predictions.

The experimentally derived residual strength ratios reported herein provide practical inputs for back-analysis and risk-informed engineering assessment of liquefaction-induced flow-type ground deformation. In a broader geotechnical hazard context, recent studies have emphasized the importance of pore-water pressure processes and mitigation-oriented assessment for stability and infrastructure performance under natural hazards [35][36].

Implications for Post-Liquefaction Stability and Relevance to the 2018 Palu Flowslide

Both low and high-fines Petobo sand specimens mobilized low normalized residual strength, confirming high susceptibility to flow-type deformation once liquefaction was triggered. Differences between fines contents were not systematic across all stress levels, reinforcing that fines content alone does not control residual strength under very loose density conditions.

The residual strength data presented in this study provide the first laboratory-based experimental reference for Petobo silty sand, helping to explain the exceptional mobility observed during the 2018 Palu flowslide and supplying essential parameters for future back-analyses, numerical modeling, and liquefaction hazard assessment in Palu and comparable alluvial environments.

Research Limitations

This study was based on six reconstituted specimens tested under monotonic consolidated undrained (CU) triaxial loading. While this approach was effective for characterizing post-liquefaction residual behavior and post-peak stress stabilization, it did not capture cyclic stress accumulation mechanisms governing liquefaction triggering during earthquakes. The use of remolded specimens prepared by moist tamping also limited representation of natural depositional fabric and stratigraphic variability in the Petobo deposits.

The tests were conducted on very loose silty sands, and extended specimen preparation required to achieve full saturation may have introduced minor uncertainties in saturation uniformity. Accordingly, the results should be interpreted as controlled laboratory observations of fundamental stress-strain response, pore-pressure generation, and residual strength under undrained monotonic loading, rather than as a comprehensive representation of in-situ field behavior.

Future research should incorporate cyclic or simple shear testing, alternative reconstitution methods, and larger datasets to improve generalization. Numerical back-analyses of the 2018 Petobo flowslide using the residual strength values obtained herein are also recommended to strengthen the linkage between laboratory-scale behavior and field-scale deformation.

CONCLUSION

This study demonstrates that loose Petobo sand is highly susceptible to liquefaction, as indicated by rapid excess pore-water pressure buildup and effective stress paths converging toward a stabilized post-peak stress condition. Although fines content influenced early-stage contractive behavior and pore-pressure generation, its effect on the ultimate post-liquefaction resistance was limited. The normalized residual strength ratios for both fines levels fell within a narrow range (q_{res}/p'_0 = 0.79 - 0.94) indicating that residual shear resistance was governed primarily by the very loose sand fabric and the effective stress level at the steady post-peak condition rather than by fines content.

These findings help clarify differences reported in previous studies regarding fines-dependent variations in post-liquefaction resistance. Under very loose initial density conditions, the influence of fines on residual strength diminished, and post-liquefaction behavior became dominated by fabric rearrangement and effective stress loss. This clarification improves the understanding of flow-failure mechanisms observed during the 2018 Petobo event and provides a clearer empirical interpretation of large-strain soil behavior.

As a preliminary investigation, this study was limited by the small number of specimens, the use of reconstituted samples, and the absence of cyclic loading. Future studies should incorporate cyclic and stress-controlled triaxial tests, evaluation of equivalent state descriptors, and coupled numerical modeling. Formal determination of the critical state line in $e\text{-}\log p'$ space and evaluation of the state parameter (ψ) are also recommended to more rigorously distinguish fines-dependent behavior within a full critical-state framework.

Overall, this study fills a critical experimental data gap for Palu by providing benchmark laboratory-based residual strength values that are directly applicable to numerical back-analysis, hazard assessment, and disaster mitigation planning. The observed steady post-peak response, which is mechanically consistent with steady-state-like or critical-state-like behavior, was used strictly as an interpretative framework for residual strength mobilization rather than as an attempt to advance critical-state theory.

ACKNOWLEDGMENT

The authors would like to thank their colleagues at the Soil Mechanics Laboratory of Parahyangan Catholic University and Universitas Mercu Buana for their technical support and valuable input during the course of this research and the preparation of this article

REFERENCE

[1] A. Jalil, T. F. Fathani, I. Satyarno, and W. Wilopo, “Liquefaction in Palu : the cause of massive mudflows,” *Geoenvironmental Disasters*, vol. 8, no. 21, pp. 1–14, 2021. doi: 10.1186/s40677-021-00194-y

[2] M. I. Tanjung, M. Irsyam, A. Sahadewa, S. Iai, T. Tobita, and H. Nawir, “Flowslide Due to Liquefaction in Petobo During the 2018 Palu Earthquake,” in *Proceedings of the 4th International Conference on Performance Based Design in Earthquake Geotechnical Engineering*, 2022, no. Beijing, pp. 565–579. doi: 10.1007/978-3-031-11898-2_33.

[3] A. P. Gallant *et al.*, “The Sibalaya flowslide initiated by the 28 September 2018 MW 7.5 Palu-Donggala, Indonesia earthquake,” *Landslides*, vol. 17, no. 8, pp. 1925–1934, 2020. doi: 10.1007/s10346-020-01354-1.

[4] R. F. Hidayat, T. Kiyota, N. Tada, and J. Hayakawa, “Reconnaissance on Liquefaction-induced Flow Failure Caused by the 2018 Mw 7 . 5 Sulawesi Earthquake , Palu , Indonesia,” *J. Eng. Technol. Sci.*, vol. 52, no. 1, pp. 51–65, 2020. doi: 10.5614/j.eng.technol.sci.2020.52.1.4

[5] L. E. Widodo, S. H. Prassetyo, G. M. Simangunsong, and I. Iskandar, “Role of the confined aquifer in the mechanism of soil liquefaction due to the 7.5 Mw earthquake in Palu (Indonesia) on 28 September 2018,” *Hydrogeol. J.*, vol. 30, no. 6, pp. 1877–1898, 2022. doi: 10.1007/s10040-022-02516-2

[6] T. C. Upomo, M. Chang, R. Kusumawardani, G. A. Prayitno, C.-P. Kuo, and U. Nugroho, “Assessment of Petobo Flowslide Induced by

Soil Liquefaction during 2018 Palu–Donggala Indonesian Earthquake," *Sustainability*, vol. 15, no. 6, p. 5371, Mar. 2023. doi: 10.3390/su15065371.

[7] T. Kiyota, M. Shiga, K. Mori, T. Katagiri, H. Furuichi, and H. Setiawan, "Triggering mechanism of long-distance flow-type landslides caused by 2018 Sulawesi Earthquake, Indonesia," *Soils Found.*, vol. 65, no. 1, p. 101544, Feb. 2025. doi: 10.1016/j.sandf.2024.101544

[8] T. Kiyota, H. Furuichi, R. Faris, N. Tada, and H. Nawir, "Overview of long-distance flow-slide caused by the 2018 Sulawesi earthquake, Indonesia," *Soils Found.*, vol. 60, no. 3, pp. 722–735, 2020. doi: 10.1016/j.sandf.2020.03.015

[9] A. Sadrekarimi, "Forewarning of Static Liquefaction Landslides," *J. Geotech. Geoenvironmental Eng.*, vol. 146, no. 9, 2020. doi: 10.1061/(ASCE)GT.1943-5606.0002320.

[10] S. Ben-Zeev, L. Goren, R. Toussaint, and E. Aharonov, "Drainage explains soil liquefaction beyond the earthquake near-field," *Nat. Commun.*, vol. 14, no. 1, pp. 1–14, 2023. doi: 10.1061/(ASCE)GT.1943-5606.0002320.

[11] D. Vidayanti, R. Nazir, D. Komerdevi, and P. T. Simatupang, "Evaluation of liquefaction potential in reworked volcanic-colluvial deposits of the Bawen Area, Semarang Regency," *Teknisia*, vol. 30, no. 2, pp. 60–72, 2025. doi:10.20885/teknisia.vol30.iss2.art1

[12] T. Kokusho, "Earthquake-induced flow liquefaction in fines-containing sands under initial shear stress by lab tests and its implication in case histories," *Soil Dyn. Earthq. Eng.*, vol. 130, no. November 2019, p. 105984, Mar. 2020. doi: 10.1016/j.soildyn.2019.

[13] H. Saeed, Z. Nalbantoglu, and E. Uygar, "Liquefaction susceptibility of beach sand containing plastic fines," *Mar. Georesources Geotechnol.*, vol. 41, no. 1, pp. 1–13, 2023. doi: 10.1080/1064119x.2021.2007556.

[14] Z. Li, S. Escoffier, and P. Audrain, "Study on the effects of a low amount of non-plastic fines on soil liquefaction by dynamic centrifuge modeling," *Soil Dyn. Earthq. Eng.*, vol. 195, p. 109400, Aug. 2025. doi: 10.1016/j.soildyn.2025.109400.

[15] M. Goudarzy, D. Sarkar, and T. Wichtmann, "Influence of plastic fines content on the liquefaction susceptibility of sands: cyclic loading," *Acta Geotech.*, vol. 17, no. 11, pp. 4977–4988, 2022. doi: 10.1007/s11440-022-01633-2.

[16] L. Jradi, B. S. El Dine, J. C. Dupla, and J. Canou, "Influence of low fines content on the liquefaction resistance of sands," *Eur. J. Environ. Civ. Eng.*, vol. 26, no. 12, pp. 6012–6031, 2022. doi: 10.1080/19648189.2021.1927195.

[17] M. A. ElGhoraiby, H. Park, and M. T. Manzari, "Stress-strain behavior and liquefaction strength characteristics of Ottawa F65 sand," *Soil Dyn. Earthq. Eng.*, vol. 138, p. 106292, 2020. doi: 10.1016/j.soildyn.2020.106292.

[18] Y. Liu, X. Wang, and P. Yu, "Critical state of granular materials at mesoscale: Transition from local to global," *Int. J. Numer. Anal. Methods Geomech.*, vol. 44, no. 12, pp. 1676–1694, 2020. doi: 10.1002/nag.3084.

[19] S. Gobbi, P. Reiffsteck, L. Lenti, M. P. S. d'Avila, and J. F. Semblat, "Liquefaction triggering in silty sands: effects of non-plastic fines and mixture-packing conditions," *Acta Geotech.*, vol. 17, no. 2, pp. 391–410, 2022. doi: 10.1016/j.soildyn.2022.107349.

[20] V. S. Quinteros and J. A. H. Carraro, "The initial fabric of undisturbed and reconstituted fluvial sand," *Geotechnique*, vol. 73, no. 1, pp. 1–15, 2023. doi: 10.1680/jgeot.20.P.121.

[21] H. Artati, W. Pawirodikromo, P. Rahardjo, and L. Makrup, "Effect of Fines Content on Liquefaction Resistance During Steady-State Conditions," *Int. J. GEOMATE*, vol. 25, no. 109, pp. 18–28, 2023. doi: 10.21660/2023.109.3481.

[22] C. Xu, C. Yue, X. Du, K. Liang, B. Wang, and G. Chen, "Experimental study on the influence of cyclic loading frequency on liquefaction characteristics of saturated sand," *Géotechnique*, vol. 75, no. 4, pp. 501–514, Apr. 2025. doi:10.1680/jgeot.21.00384.

[23] C. P. Polito, J. R. Martin, and E. L. D. Sibley, "The Effect of Non-Plastic Fines Content on Pore Pressure Generation Rates in Cyclic Triaxial and Cyclic Direct Simple Shear Tests," *Eng*, vol. 5, no. 4, pp. 2410–2427, 2024. doi: 10.3390/eng5040126.

[24] K. . Tran, S. Imanzadeh, S. Taibi, H. Souli, J. . Fleureau, and M. Hattab, "Effect of saturation on liquefaction potential and residual strength: laboratory investigation," *Eur. J. Environ. Civ. Eng.*, vol. 26, no. 15, pp. 7480–7502, 2022. doi: 10.1080/19648189.2021.1999333.

[25] R. E. S. Moss, D. Ph, and F. Asce, "Liquefied Strength and Its Relationship to Effective Stress," *J. Geotech. Geoenvironmental Eng.*, vol. 146, no. 2015, pp. 1–6, 2020. doi: 10.1061/ (ASCE)GT.1943-5606.0002391.

[26] I. D. Gates and M. Ghayoomi, "Residual

Strength of Liquefied Soil: The Effect of Induced Partial Saturation," *Geotech. Test. J.*, vol. 45, no. 4, pp. 855–876, Jul. 2022, doi: 10.1520/GTJ20210217.

[27] M. V Manmatharajan, S. Gill, W. Liu, E.-P. Ingabire, A. Sy, and M. Ghafghazi, "Effect of particle size and particle size distribution on critical state loci of granular soils," *Can. Geotech. J.*, vol. 60, no. 8, pp. 1117–1131, 2023. doi: 10.1139/cgj-2021-0643

[28] R. E. S. Moss, T. R. Honnette, and J. S. Jacobs, "Large-Scale Liquefaction and Postliquefaction Shake Table Testing," *J. Geotech. Geoenvironmental Eng.*, vol. 146, no. 12, p. 04020138, 2020. doi: 10.1061/(ASCE)GT.1943-5606.0002400

[29] S. Ocak and K. O. Cetin, "Liquefaction-Induced Failure of Demirköprü Bridge Pile Foundation and Retaining System. Following the February 6 Kahramanmaraş Earthquake Sequence," *J. Earthq. Eng.*, vol. 29, no. 16, pp. 3505–3519, 2025. doi: 10.1007/s10518-024-01875-3.

[30] R. Verdugo, "Static liquefaction in the context of steady state/critical state and its application in the stability of tailings dams," *Soil Dyn. Earthq. Eng.*, vol. 176, no. 1, p. 108270, 2024. doi: 10.1016/j.soildyn.2023.108270

[31] P. Li, C. Zhu, X. Pan, B. Lv, and K. Pan, "Undrained shear behavior of silty sand with a constant state parameter considering initial stress anisotropy effect," *Sci. Rep.*, vol. 14, p. 2213, 2024, doi: 10.1038/s41598-023-50901-y

[32] A. Papadopoulou and T. Tika, "Monotonic and cyclic behaviour of sand-silt mixtures through the equivalent state parameter," in *E3S Web of Conferences*, 2024, p. 14014. doi: 10.1051/e3sconf/202454414014

[33] A. V. da Fonseca, D. Cordeiro, and F. Molina-Gómez, "Recommended Procedures to Assess Critical State Locus from Triaxial Tests in Cohesionless Remoulded Samples," *Geotechnics*, vol. 1, no. 1, pp. 95–127, 2021. doi: 10.3390/geotechnics1010006

[34] T. Sasaki, S. Kawamura, and J. Koseki, "Liquefaction Properties of Two Types of Sandy Soil Specimens with Different Compaction Thickness," in *Advances in Innovative Geotechnical Engineering (GeoChina 2021)*, 2021, pp. 19–30. doi: 10.1007/978-3-030-80316-2_3

[35] N. Gofar, E. N. Pangestika, Y. Harianto, H. Gumay, and A. Satyanaga, "Effect of near-surface heterogeneities on the pore-water pressure distribution and slope stability," *SINERGI*, vol. 28, no. 2, pp. 327–336, 2024. doi: 10.22441/sinergi.2024.2.012

[36] A. I. Rifai, J. Prasetijo, M. Isradi, Y. A. Sari, and M. F. Zolkipli, "Flood and landslide exposure awareness for mitigation of road network performance : a community-based approach," *SINERGI*, vol. 29, no. 2, pp. 411–422, 2025. doi: 10.22441/sinergi.2025.2.012